41th ERF, September 1–4, 2015, Munich, Germany

017

A Test Rig to Assess the Effectiveness of Drag Reduction Devices on a Heavy-Class Helicopter

G. Gibertini*[1], F. Auteri[1], G. Campanardi[1], G. Droandi[1], D. Grassi[1], A. Le Pape[2] and A. Zanotti[1]

[1]Politecnico di Milano – Dipartimento di Scienze e Tecnologie Aerospaziali
Via La Masa 34, 20156 Milano – Italy
[2]ONERA – The French Aerospace Lab – Applied Aerodynamics Department
8, Rue des Vertugadins, F-92190 Meudon – France
e–mail: *giuseppe.gibertini@polimi.it

Keywords: Drag reduction, Helicopter, Wind Tunnel.

Abstract

The present paper describes the experimental activity carried out to evaluate the effectiveness of the CFD-based shape optimisation of several components of a common helicopter platform of the heavy-weight class. The considered geometry is basically the same of the model tested in the frame of the GOAHEAD project. The comprehensive wind tunnel campaign includes both the original helicopter configuration and the optimised version to assess the optimisation effectiveness by comparison. The optimised components included different hub-cap configurations, a set of fairings for the blade-stubs attachments and the sponsons. Moreover, the effects on drag reduction produced by an array of vortex generators positioned on the back-ramp were investigated. Different measurement techniques were employed as loads and moments measurements, steady and unsteady pressure surveys and stereo particle image velocimetry. The performed measurements confirm a overall drag reduction of about 6% at cruise attitude for the optimised configuration.

Nomenclature

C_D	drag coefficient
C_{D0}	drag coefficient measured for the baseline upright model with rotating hub
C_p	pressure coefficient
p	Kulite pressure signal
$\langle p \rangle$	mean of the Kulite pressure signal
Ma	Mach number
PIV	Particle Image Velocimetry
t	acquisition time
U_∞	free-stream velocity [m/s]
VG	Vortex Generators
X	stream-wise coordinate [m]
Y	span-wise coordinate [m]
Z	vertical coordinate [m]
u	stream-wise velocity component [m/s]
α	angle of attack [deg]
ψ	azimuthal blade angle [deg]
ω	rotor hub rotational speed [RPM]

1 Introduction

The problem of the environmental impact has become in the recent years particularly serious due to the expansion of the helicopter use. Therefore, the optimisation of helicopter shape for drag reduction represents an important research topic to obtain a reduction of fuel consumption. For these reasons, the investigation of drag reduction devices was then introduced in the work plan of the GRC (Green RotorCraft) project in the frame of Clean Sky programme.

The present paper describes the wind tunnel tests carried out in the frame of the Clean Sky ROD project. The aim of the tests was to evaluate the effectiveness of the CFD-based shape optimisation performed by GRC2 consortium on several components (i.e. hub-cap [1], blade attachments, sponsons, back ramp area [2]) of a common helicopter platform of the heavy-weight class. The model employed for the present activity was basically the same one tested in the frame of GOAHEAD project [3] funded by EU's Sixth Framework Programme for Research (FP6). In particular, the model internal structure, the motorised horizontal stabilizer and the swash-plate were re-designed and built purposely for this test campaign. The tests were carried out in the large wind tunnel of Politecnico di Milano (GVPM). A comprehensive experimental campaign was carried out including both the original helicopter configuration and the optimised version. The tested optimised components were two different hub-caps, a set of fairings for the blade-stub attachments and a new set of sponsons. Moreover, the effect of vortex generators on the back ramp area was investigated with the model upside-down in order to avoid pylon wake interference.

Different measurement techniques were employed in the wind tunnel activity. Both the global and the partial airloads acting on the rotating rotor hub equipped with blade stubs were measured. Steady pressure measurements were performed over more than 300 points located over the fuselage and the horizontal stabilizer. The back-ramp and the fin of the model were instrumented with fast-response pressure transducers. Stereo PIV surveys were performed on several longitudinal planes above the back-ramp and in the area before the fin to investigate respectively the effect of the vortex generators on the three-dimensional flow field and the pattern of the rotor wake with the different hub-caps tested.

The paper describes in details the test rig, the measurements performed and the main results of the experimental activity carried out on both original and optimised configurations which allowed to confirm a overall drag reduction of about 6% at cruise attitude.

2 Experimental Set up

The wind tunnel tests were carried out in the large wind tunnel (GVPM) of Politecnico di Milano (POLIMI). The wind tunnel has a 4 m × 3.84 m test section. The maximum wind velocity is 55 m/s and the turbulence intensity is less than 0.1%.

2.1 The helicopter model

The helicopter model in 1/4 scale was set up for the wind tunnel activity by POLIMI. In particular, the model set up starts from some pre-existing components. Indeed, the fuselage was the same used for the GOAHEAD project [3]. The layout of the new structure of the helicopter model is shown in Fig. 1.

The swash-plate and additional sponsons were purposely designed and built for these tests. Only the motorised horizontal stabiliser was designed and built by LMS and NLR [4]. The fully articulated rotor hub, provided by NLR, was equipped with blade stubs. The collective, longitudinal and lateral pitch of the blade stubs can be set by three electric actuators acting on the swashplate. The rotor was driven by a brushless motor with a 5:1 geardrive. A Hall Effect sensor was mounted on the rotor hub to measure the 1/rev of the master blade. The internal metallic structure was re-designed and built in order to interface the model in both upright and upside-down configuration with the GVPM strut that is fixed to the test section floor. The model was attached to the head of the strut allowing to set the angle of attack. A turning-table on the test-section floor allowed to set the model sideslip angle. The upside-down tests were especially addressed to evaluate the performance of the vortex generators (VG) array and of the optimised sponsons. Indeed, for the upside-down tests the head of the strut was fixed to the helicopter upper side so that the flow around the model back-ramp was not disturbed by the wake of the strut.

2.2 The optimised components

The assessment of the optimised components for drag reduction included tests on two different hub-caps, a set of fairings for blade stubs attachments, a set of new sponsons and different configurations of VG array. POLIMI designed and manufactured these components starting from the shapes optimised from ONERA and DLR by means of CFD.

In particular, ONERA provided the shape of a hub-cap and of the blade stubs attachments fairings. Namely, this hub-cap and farings will be respectively called in the following small hub-cap and stubs fairings (see Fig. 2(a)). The second hub-cap tested was manufactured starting from the external optimised shape of a full hub fairing optimised by DLR [1]. Differently from the original design by DLR, this component presents a large open underside necessary to avoid interference with the actual rotor hub. Namely, in the following this hub-cap (see Fig. 2(b)) will be called large hub-cap. DLR provided also the shape of the optimised set of sponsons (see Fig. 2(c), namely new sponsons).

The present test activity investigated also the effect in terms of drag reduction of four set of co- and counter-rotating VG arrays positioned on the back-ramp area (see the best configuration illustrated in Fig. 2(d)). The dimensions and the position of the VG were optimised by ONERA as described in the work by Boniface [2].

2.3 Airloads measurements

The global aerodynamic loads and moments were measured by a six-component RUAG 192-6L strain-gauge internal balance installed on the head of the strut. The partial loads and moments acting on the rotor hub equipped with blade stubs were measured by a six-components RUAG 196-6D strain-gauge balance installed inside the model (see Fig. 1). The motorised horizontal stabiliser was also instrumented with a two-components strain-gauge balance to measure the vertical component of the aerodynamic load and the rolling moment.

2.4 Pressure measurements

More than three-hundred static pressure taps are distributed on the model fuselage and on the horizontal stabiliser. The sponsons are not equipped with pressure taps. The static pressure measurements were carried out by means of 8 pressure scanners (1 PSI F.S., accuracy 0.1% F.S.) embedded inside the model. The back-ramp and the fin of the model were instrumented with twenty XCS-093 Kulite miniature fast-response pressure transducers (2 PSI F.S., accuracy 0.1% F.S.). The position of the pressure taps on the model surface for both the steady and unsteady measurements is illustrated in Fig. 3, showing also the X-Y-Z refence system employed in this paper.

The pressure signals were acquired for 10 s for each model attitude. The Kulite transducers signals were acquired simultaneously with the Hall-Effect sensor signal to reconstruct the

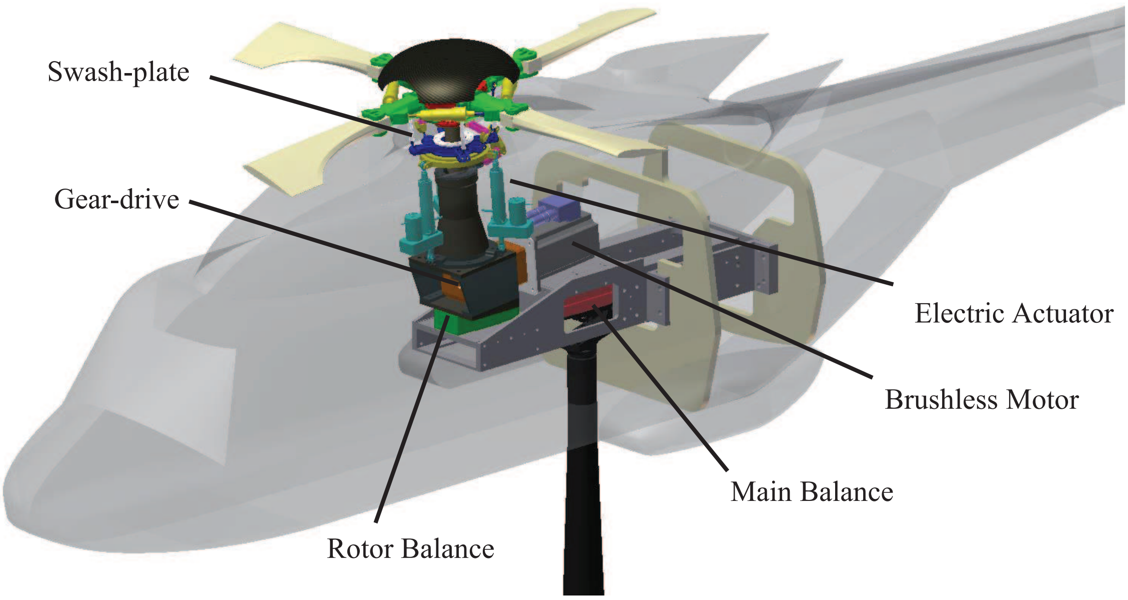

Figure 1: Layout of the helicopter model.

instantaneous azimuthal position of the master blade during unsteady pressure measurements.

2.5 PIV set up

Stereo PIV surveys were carried out in two different areas. For the upside-down configuration tests, the measurement area was located in the region at the junction between the rear ramp and the tail boom to investigate the effect of the VG. For the upright configuration tests, the measurement area was located just ahead the fin to investigate the rotor wake with the different hub-caps. The system was set up to measure the three velocity components on longitudinal X-Z plane windows at different span-wise locations. This technique enables to reconstruct the mean three-dimensional flow over a volume [5]. The surveys were carried out over a range of 260 mm centered on the model mid-span section. The spacing between the measurement planes in span-wise direction was 5 mm for the surveys over the back-ramp region (total number of 53 measurement planes). For the upright tests, the spacing between the measurement plane was increased to 10 mm (total number of 27 measurement planes) to obtain an admissible run time with the rotating hub. The measurement windows area was respectively 365 mm $\times$ 185 mm in the back-ramp region and 157 mm $\times$ 310 mm ahead the fin. The position of the measurement volumes is illustrated in Fig. 4. A set of 100 image pairs was acquired for each measurement plane.

The layout of the PIV instrumentation is shown in Fig. 5. The PIV system consisted of a Litron NANO-L-200-15 Nd:Yag double pulsed laser with a 200 mJ output energy and a wavelength of 532 nm, and two Imperx ICL-B1921M CCD cameras with a 12 bit, 1952 $\times$ 1112 pixel array. The laser was mounted on a single-axis traversing system positioned on the ceiling of the wind tunnel test section. The cameras were moved in the span-wise direction by means of two linear guides attached on a metallic strut. The metallic strut, attached on the side wall of the test section, enabled to rotate the cameras around the model rotation point to easily adjust the image views with respect to the model angle of attack selected for the PIV survey. Each camera was equipped with a Nikkor 50 mm lens and tilting lens mountings to achieve the Schleimpflug condition. The camera separation angle was set to 40° to obtain a correct optical access to the measurement area. The laser and the cameras were moved simultaneously in span-wise direction to have for each measurement plane a correct focusing of the

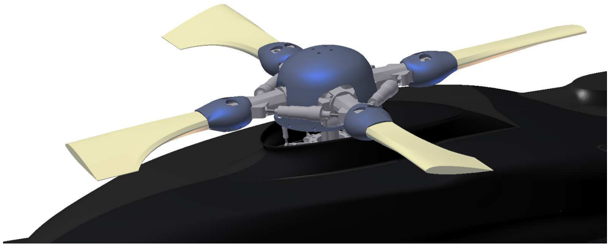

(a) Small hub-cap + blade stubs fairings designed from ONERA CFD-based shape optimisation

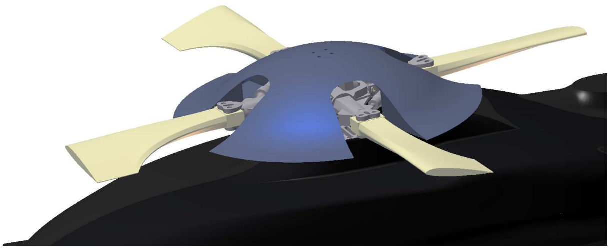

(b) Large hub-cap designed from DLR CFD-based shape optimisation

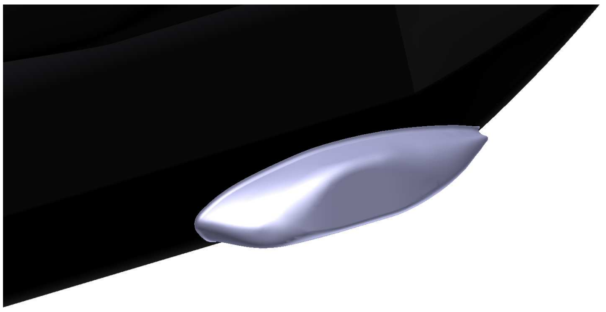

(c) New sponsons from DLR CFD-based shape optimisation

(d) Counter-rotating VG array designed from ONERA CFD optimisation

Figure 2: Optimised components tested in wind tunnel.

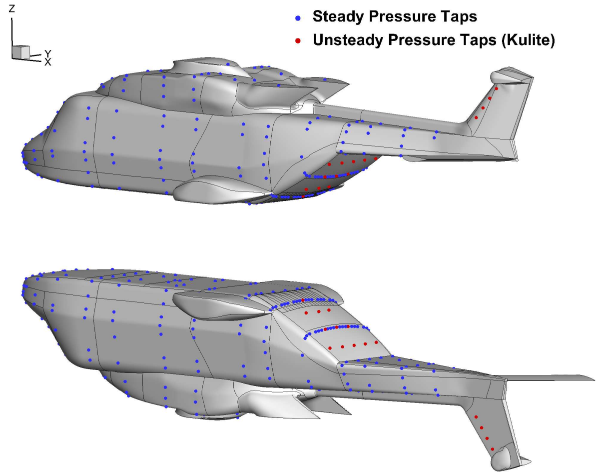

Figure 3: Layout of the pressure taps distribution on the model surface.

laser sheet with the image plane. The synchronization of the two laser pulses with the image-pair exposure was controlled by a 6-channel Quantum Composer QC9618 pulse generator. The acquisition of the image pairs for the surveys in upright configuration with the rotating hub was phase-locked with a prescribed azimuthal position of the blade stub ($\psi = 0°$ corresponds to the master blade axis aligned with the fuselage mid-span plane). A particle generator with Laskin atomizer nozzles was used for the seeding of the entire test-section. The particles consisted of small oil droplets with a diameter in the range of 1-2 μm.

The image-pair analysis was carried out by the PIVview 3C software [7], developed by PIVTEC. In particular, the multigrid interrogation method [6] was used starting from a 96 pixels $\times$ 96 pixel to a 32 pixel $\times$ 32 pixel interrogation window. The accuracy of the PIV measurement can be estimated considering a maximum displacement error of 0.1 px [5]. Thus, considering the employed pulse-separation time and the optical magnification, the maximum error for the in-plane velocity components results to be about 1% of the maximum in-plane velocity component [8]. Due to the stereoscopic optical set-up, a slightly higher error can be estimated for the out-of-plane velocity component.

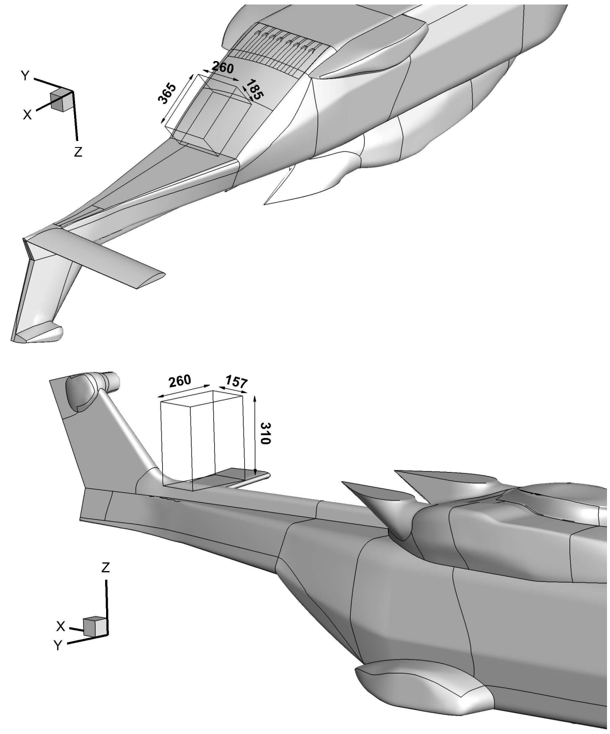

Figure 4: PIV measurement volumes on the back ramp and ahead of the fin, dimensions in mm.

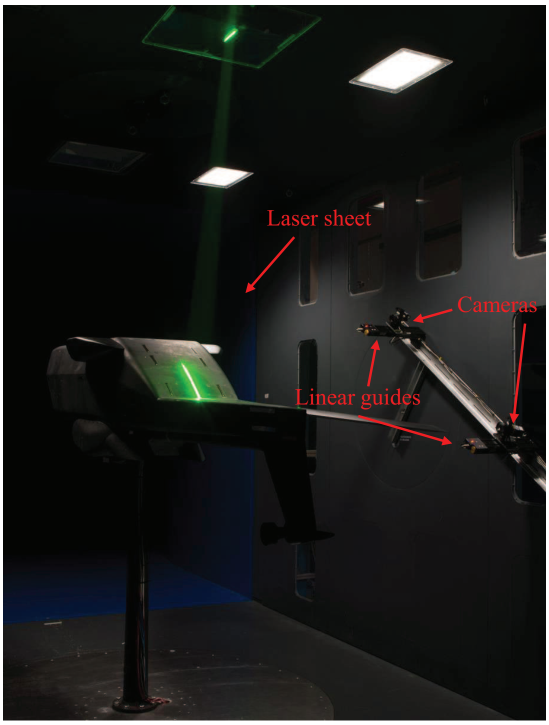

Figure 5: Layout of the PIV instrumentation in the wind tunnel test section.

3 Results

The present section describes the main results of the tests carried out with the model in both upright and upside-down configuration. The maximum wind tunnel free-stream velocity during the tests was 50 m/s ($Ma = 0.15$). All the presented data are corrected considering the wind tunnel effects. In particular, the data were corrected for the strut interference, the horizontal buoyancy in the test section and the model solid blockage.

Figure 6: The helicopter model mounted upside-down in the GVPM wind tunnel at POLIMI.

The tests with the model in upside-down configuration (see Fig. 6) were addressed to evaluate the performance of the best VG array and of the optimised sponsons avoiding the interference of the strut wake. The drag measurements carried out with the model at cruise angle of attack showed that the smaller counter-rotating VG array provides the higher drag reduction. Therefore, this VG configuration was investigated in details in the wind tunnel campaign.

Figure 7 shows the comparison between the drag coefficients measured with the baseline model (with the original sponsons) and with the model equipped with the best VG array and the new sponsons. In particular, the tests were carried out adding the components to evaluate their own contribution to drag reduction. The test results show that at $\alpha = -2°$ the best VG array on the back ramp produces a reduction of 1.8% of the drag measured in upright configuration for the baseline model with rotating hub. The optimised sponsons produces a fur-

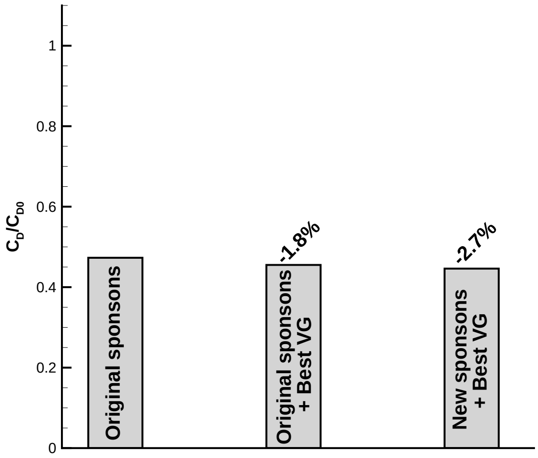

Figure 7: Effect on drag of the best VG array and new sponsons measured for the upside-down configuration at $\alpha = -2°$, $Ma = 0.15$: the indicated percentual C_D differences are referred to C_D measured at the same angle of attack in upright configuration for the baseline model with rotating hub.

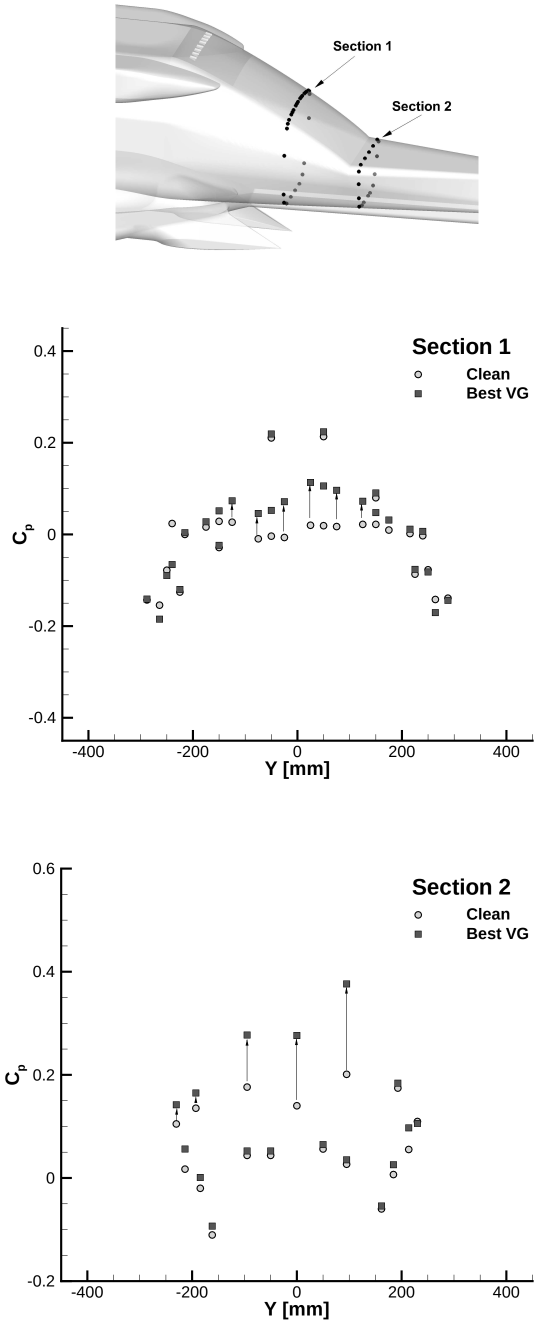

Figure 8: Effect of the best VG on C_p distribution at selected fuselage sections for the tests in upside-down configuration, $\alpha = -1.8°$, $Ma = 0.15$.

ther drag reduction of 0.9%.

Static pressure measurements and PIV surveys enabled to achieve a detailed insight about the physics related to the functioning of the VG array. In particular, Fig. 8 shows the comparison of the mean C_p distribution measured over two selected sections with and without the VG. A clear increase of pressure on the back-door surface is observed with the VG for both the considered instrumented sections, as indicated by the arrows oriented upwards. Thus, static pressure measurements confirm the benefit of VG in reducing drag obtained by limiting the suction effect responsible for pressure drag rise. Moreover, VG are responsible of re-energising the boundary layer, thus preventing or limiting flow separation. This effect is clearly visible from the comparison between the PIV velocity field measured in the back-ramp region with and without the VG.

Figure 9 shows the comparison of the averaged non-dimensional stream-wise velocity component u/U_∞ illustrated on a longitudinal and on different span-wise planes extracted from the measurement volume. For the clean geometry configuration (without the VG), the flow close to the ramp is characterised by a large separation. The extent of this separated flow region in both longitudinal and span-wise direction is clearly indicated by the negative values of the stream-wise velocity component measured on $X - Z$ and $Y - Z$ planes. On the other hand, PIV surveys carried out with the model equipped with the VG do not show back-flow region in the volume of investigation.

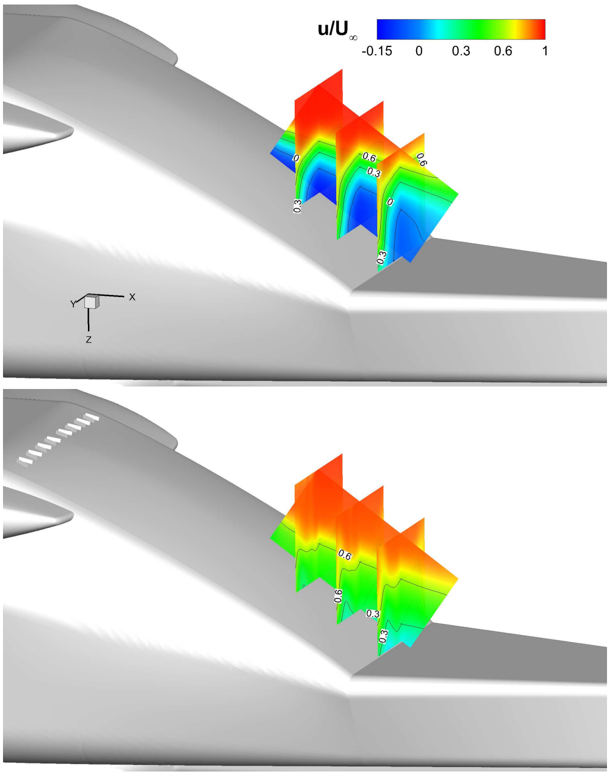

Figure 9: Effect of the best VG on the velocity field in the back-ramp region: PIV results for the tests in upside-down configuration at $\alpha = -1.8°$, $Ma = 0.15$.

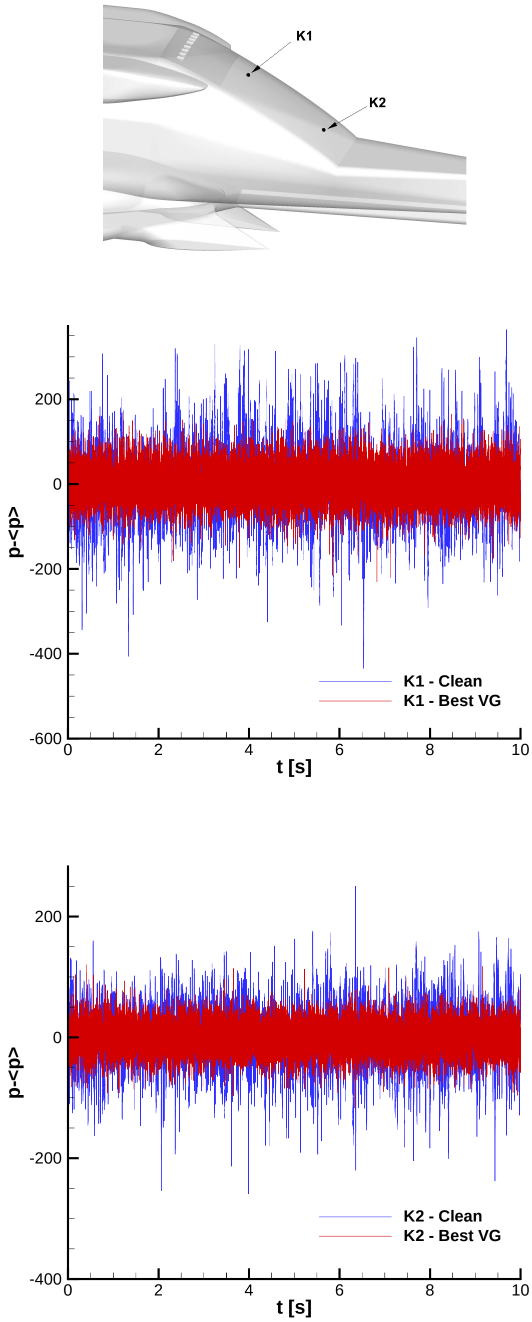

Figure 10: Kulite pressure signals with and without VG for the tests in upside-down configuration, $\alpha = -1.8°$, $Ma = 0.15$.

The unsteady pressure measurements carried out over the back-ramp surface provide a comparison of the unsteadiness level of the flow in this region between the clean geometry case and the model configuration with the VG. Figure 10 show the comparison of the pressure time-histories measured by two Kulite transducers located on the mid-span plane of the back-ramp downstream the VG array. In order to highlight the comparison of the pressure fluctuations with and without the VG, the difference between the measured pressure signals and their mean values are plotted on the same graph for each transducer. Coherently with the velocity field surveys, the measurements carried out with the clean geometry show a rather higher level of pressure fluctuations, confirming the higher level of unsteadiness that characterise the separated flow region without the VG.

The tests with the model in upright configuration with the rotating hub were mainly addressed to evaluate the performance of the different optimised hub configuration in terms of drag reduction. In order to obtain an accurate estimate of the contribution to the aerodynamic performance, the tests were performed by adding all the optimised components starting from the original to the final optimised configuration. During the tests, the rotational speed of the rotor hub was $\omega = 710$ RPM. Figure 11 shows the helicopter model mounted upright in the wind tunnel test section in the original and optimised configuration.

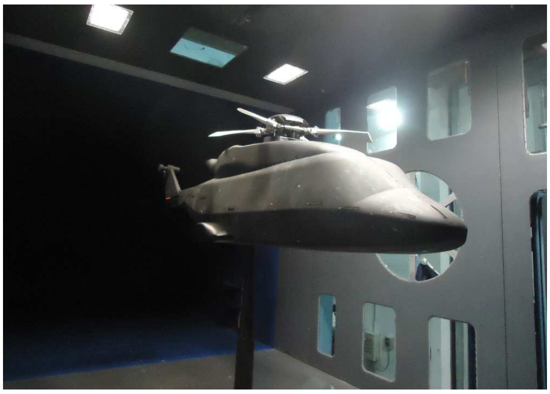

(a) Original configuration

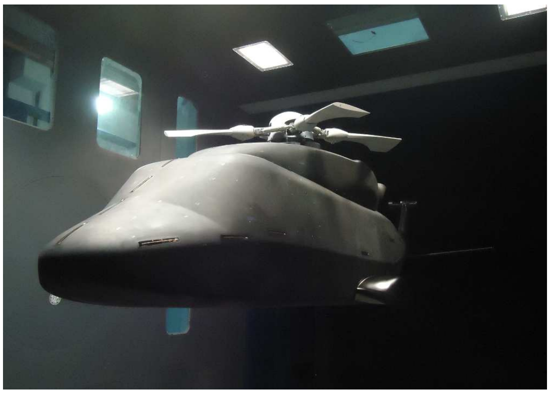

(b) Optimised configuration: small hub-cap, blade stubs fairings, new sponsons, array of VG in the back-door region

Figure 11: The helicopter model mounted upright in the GVPM wind tunnel at POLIMI.

Figure 12 shows the drag coefficients measured at $\alpha = -2°$ for the different configurations tested. In particular, the contribution of the different optimised components are indicated in terms of percentual drag differences calculated with respect to the measurement carried out with the original model geometry. As the measurements indicate that the performance of the VG and of the new sponsons is clearly influenced by the strut wake, the drag coefficients reported in Fig. 12 were corrected for the struct interference effect taking into account the upside-down measurements.

The best performance between the hub-caps was found with the small hub-cap. The blade stubs attachments fairings produce a small increase of the performance with the small hub-cap, while they produce a contained decrease of the large hub-cap. Therefore, the wind tunnel activity showed that an overall maximum drag reduction of 6.1% can be obtained at cruise attitude with respect to the original geometry.

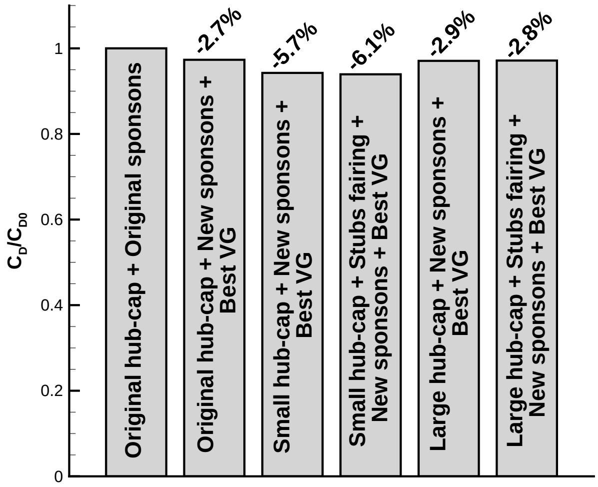

Figure 12: Effect on drag of the different hub-caps and stubs fairings measured for the upright configuration with the rotating hub, $\alpha = -2°$, $Ma = 0.15$, $\omega = 710$ RPM: the percentual C_D differences are referred to C_D measured in upright configuration tests for the baseline model with rotating hub.

The design of the hub-cap should be optimised to deflect the rotor hub wake in order to avoid the impact on the fin. Thus, PIV surveys were carried out to investigate the effect of the different optimised hub-caps on the rotor hub wake just before the fin. The comparison of the phase-averaged PIV results obtained with the original and optimised hub-cap components at cruise angle of attack are illustrated in Fig. 13, showing the contours of the non-dimensional stream-wise velocity component u/U_∞ on a longitudinal and span-wise plane extracted from the measurement volume. PIV results for the original hub-cap configuration show that the velocity defect region is confined in the lower part of the measurement volume close to the tail boom. Thus, the rotor hub wake influences only the lowest part of the fin. On the other hand, a wider velocity defect region can be observed from the PIV results obtained with both the large and small opti-

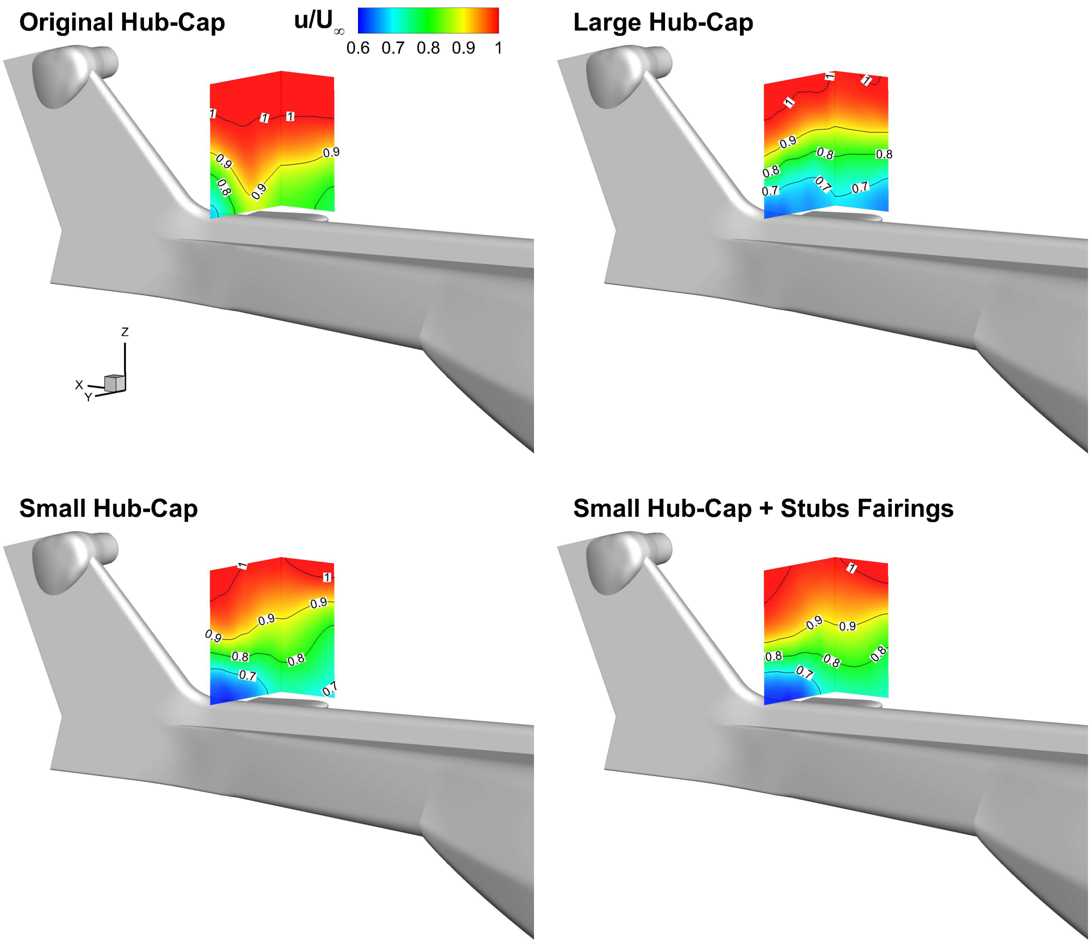

Figure 13: Effect of the hub-caps on the rotor hub wake: phase averaged PIV results for the tests in upright configuration at $\alpha = -1.8°$, $Ma = 0.15$, $\omega = 710$ RPM, $\psi = 0°$.

mised hub-caps. In particular, the area with the higher velocity defect is more extended for the large hub-cap configuration. Thus, both these components produce a rotor hub wake that strokes about half of the fin span. Moreover, the blade stubs attachments fairings do not produce appreciable effects on the rotor hub wake.

4 Conclusions

A comprehensive experimental activity was carried out to assess the effectiveness of CFD-based optimised components for the reduction of helicopter drag. In particular, an heavy-class helicopter model was set up to be tested in the POLIMI wind tunnel. An accurate evaluation of the performance of different hub-caps, a set of blade stubs attachments fairings and a new set of sponsons was performed by means of aerodynamic loads and moments measurements. Moreover, the effectivess of vortex generators located on the model back-ramp was investigated. Wind tunnel measurements confirm the effectiveness of the optimised components showing an overall drag reduction of about 6% at cruise attitude. Moreover, steady and unsteady pressure measurements and stereo PIV survey enabled to achieve a detailed insight about the flow physics related to the use of VG and about the behaviour of the rotor wake for the hub configurations with the different optimised hub-caps.

Acknowledgements

The research leading to these results has received funding from the European Community's Seventh Framework Programme (FP7/2007-2013) for the Clean Sky Joint Technology Initiative under grant agreement n. 325997.

References

[1] Khier W. Computational Investigation of Advanced Hub Fairing Configurations to Reduce Helicoper Drag, *40th European Rotorcraft Forum*, Southampton, UK, 2-5 September, 2014.

[2] Boniface JC. A Computational Framework for Helicopter Fuselage Drag Reduction Using Vortex Generators. *American Helicopter Society 70th Annual Forum*, Montreal, Quebec, Canada, 20-22 May 2014.

[3] Raffel M., De Gregorio F., Groot K.D., Schneider O., Sheng W., Gibertini G. and Seraudie A. On the generation of a helicopter aerodynamic database. *Aeronautical Journal*, Vol. 115, pp 103-112, 2011.

[4] Lemmens Y., Decours J., Fijalek M. and Hakkart J. Development of Active Horizontal Stabilizer, *38th European Rotorcraft Forum*, Amsterdam, The Netherlands, 4-7 September, 2012.

[5] Zanotti A., Ermacora M., Campanardi G. and Gibertini, G. Stereo particle image velocimetry measurements of perpendicular blade vortex interaction over an oscillating airfoil. *Experiments in Fluids*, Vol. 55, N. 9, 1811, pp 1-13, 2014.

[6] Raffel M., Willert C., Wereley S. and Kompenhans J. Particle Image Velocimetry - A Practical Guide, Springer Verlag, Berlin, 2007.

[7] PIVview 2C/3C, User Manual, PIVTEC, www.pivtec.com, 2010.

[8] De Gregorio F., Pengel K. and Kindler K. A comprehensive PIV measurement campaign on a fully equipped helicopter model. *Experiments in Fluids*, Vol. 53, pp. 37-49, 2012.